Research Article Vol. 3, No. 6 / 15 Jun 2024 / Optics Continuum 983
OPTICS CONTINUUM

Demonstration of temperature monitoring of the curing process in resin transfer moulding using integrated phase-shifted Bragg grating sensors

GEORGIOS SYRIOPOULOS,[1,7,†] EVRYDIKI KYRIAZI,[1,8,†] GIANNIS POULOPOULOS,[1] THENIA PROUSALIDI,[1] AGGELOS POULIMENOS,[2] MICHAL SZAJ,[3] MIGUEL LIZARANZU,[4] JOSÉ LUIS NÚÑEZ,[4] FRANCK BOURCIER,[5] SÉBASTIEN MAUGIS,[5] JEROEN MISSINNE,[6] GEERT VAN STEENBERGE,[6] CHARALAMPOS ZERVOS,[1] AND HERCULES AVRAMOPOULOS[1]

[1]*Photonics Communications Research Laboratory, National Technical University of Athens, 9 Iroon Polytechniou Street, Zografou Athens 15773, Greece*
[2]*Engineering Technology Solutions E.E. Athens, Greece*
[3]*Argotech a.s., Holubova 978, Náchod, CZ-547 01, Czech Republic*
[4]*ITAINNOVA, María de Luna, n°7-8 (Pol. Actur), 50018, Zaragoza, Spain*
[5]*Loiretech Ingénierie, Pôle Jules Verne, 9 rue du Moulin cassé, 44340 Bouguenais, France*
[6]*Center for Microsystems Technology (CMST), Ghent University and imec, Technologiepark 126, Zwijnaarde 9052, Belgium*
[7]*georgesyriopoulos@mail.ntua.gr*
[8]*evkyriazi@mail.ntua.gr*
[†]These authors contributed equally to this work

Abstract: Composite materials have increased in use across multiple industries due to their low weight, thermal stability and design flexibility. As applications grow, the importance of accurate process-monitoring techniques grows, with various research teams investigating a variety of in situ cure-monitoring sensors. Photonic integrated circuits (PICs) can be a feasible solution in tracking curing cycles due to their resistance to harsh conditions and ease of integration into the production tool. This paper demonstrates the integration and performance evaluation of an embedded phase-shifted Bragg grating solution, instead of commonly used fiber sensors, based on 220 nm height silicon-on-insulator platform for in-situ monitoring of the RTM-6 resin curing process in a composite tool. The embedded optical sensor presents high sensitivity (75 pm/°C) and linearity (R^2=0.995) up to 120 °C, enabling precise temperature measurements throughout the curing cycle. The experimental results show consistency with previously reported simulations, throughout the calibration, dry run characterization and the curing process, up to 120 °C, allowing for accurate monitoring of the curing process.

1. Introduction

Composite materials have been widely used in various engineering fields such as aerospace, aeronautics, automotive and railways since compared to traditional metal alloys, have allowed significant weight reduction, high thermal stability and design flexibility [1]. One of the most cost-competitive manufacturing processes for composites is resin transfer moulding (RTM), in which dry reinforcement fibres are placed into a mould, then the mould is closed, and resin is injected. [2]. The in-situ measurement of RTM parameters such as temperature, injection pressure and flow rate play fundamental role for the occurrence of variations in resin properties, preform characteristics and error procedures.

#522327 https://doi.org/10.1364/OPTCON.522327
Journal © 2024 Received 27 Feb 2024; revised 29 Apr 2024; accepted 30 Apr 2024; published 10 Jun 2024

OPTICS CONTINUUM

In advanced composite applications, achieving a specified resin cure state is a critical quality objective because the completion of the polymer conversion process is directly related to the mechanical performance of the final product [3]. To capture the effects of this variability, the cure process for each individual part must be monitored. Among the most commonly used methods of tracking temperature variations, the use of thermocouples, capacitive sensors and fiber Bragg grating sensors is especially notable [4].

The electrical solutions noted above can be bulky in size, both in terms of wiring and sensors, making them difficult to embed in composite tools. More importantly, their susceptibility to electromagnetic interference and limited range makes their use in carbon fibre composite tools prohibitive [5]. Photonic structures can bridge that gap, with optical fibre configurations already deployed in sensing applications [6–8], for structural health monitoring [9,10] and especially in the composite industry [11–14]. However, these sensors are either embedded at a certain depth in the tool or the produced part, making monitoring at the tool-resin interface difficult.

In recent years, the implementation of optical sensors in integrated photonics platforms has advanced as a promising method due to their robustness to harsh environments, miniaturization potential and rapid response. Implementing optical sensors in integrated photonics platforms, yields certain advantages, namely response speed [15], immunity to electromagnetic interference [16], miniaturization potential [17,18], and ability to multiplex signals [19], while the photonic structures can be placed right on the surface of the production tool, allowing better monitoring of the resin's curing cycles.

As was previously demonstrated [20,21], photonic integrated circuits (PICs) based on 220 nm height silicon-on-insulator platform were embedded in a composite tool used to produce high quality RTM-6 composite parts. Prior work presented in [22] included the optical sensor design, the lab calibration and the in-tool characterization in a dry run setup. The present study follows this work, demonstrating a photonic sensor embedded in a composite tool, infused with a resin curing at 120 °C. Throughout the curing process, the sensor exhibits high sensitivity (75 pm/°C), high linearity (R2 = 0.995), and operating up to the curing cycle of the resin. We illustrate the experimental curing process by injecting RTM-6 resin into a composite tool comparing the precise temperature data of the optical sensors under test with that of the electrical sensors (thermocouples) which enables the real-time temperature monitoring across the curing cycle.

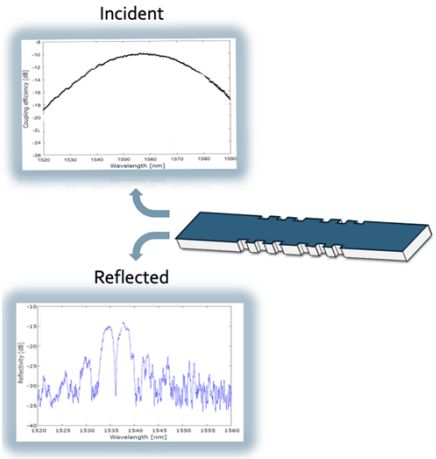

Fig. 1. Schematic of a phase-shifted Bragg grating structure and its reflection spectrum.

OPTICS CONTINUUM

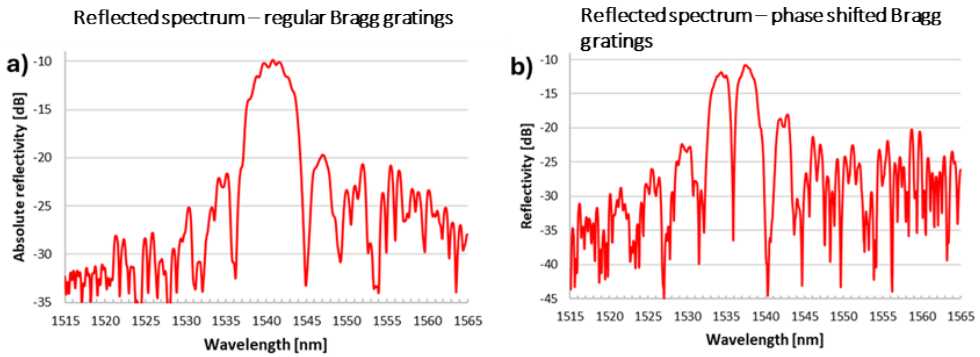

Fig. 2. Reflection spectrum comparison between a regular Bragg grating (a), and a phase shifted one (b), fabricated on a silicon photonics platform.

2. Materials and methods

2.1. Integrated Bragg grating structure

The optical structure chosen for the implementation of the sensor, is a Bragg grating, created through the periodic corrugation of a silicon waveguide's sidewall. Due to this periodicity in the structure, a part of the radiation spectrum is reflected, with the response being highly dependent on the temperature, as the rise in temperature causing a red-shift in the reflection spectrum. As the temperature change is tracked using the central wavelength of the reflection lobe, it is imperative to reduce the bandwidth of this lobe, for an increase in accuracy. This is achieved with the use of a phase shift, i.e. an uncorrugated period, right at the center of the structure. This causes a narrow dip at the reflection lobe, allowing for an accurate tracking of the temperature variations. Figure 1 presents the operating principle of an integrated Bragg grating, with the incident and reflected radiation also visible.

The difference in the reflection spectrum between a regular and a phase shifted Bragg grating, can be seen in Fig. 2. As the dip of the phase shifted structure has a much narrower bandwidth than the lobe of the regular structure, the accuracy in temperature tracking is increased.

As presented in [20,21], the sensor is fabricated on a 220 nm silicon on insulator platform, using a multi-project wafer (MPW) service by IMEC, specifically the iSiPP50 G platform [23]. After fabrication, the sensor PICs were coupled with an optical fiber and packed in a protective

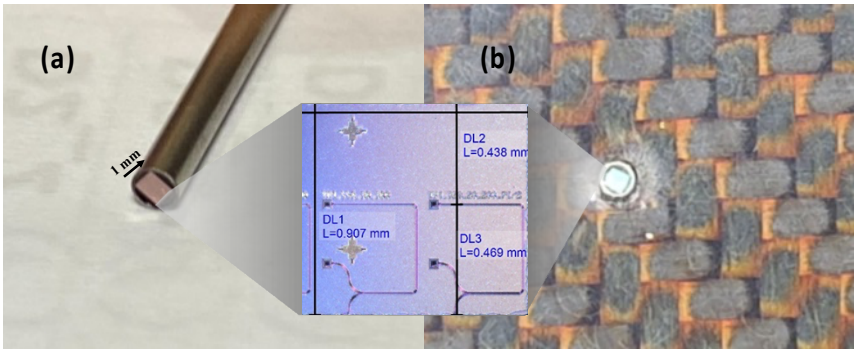

Fig. 3. (a) The packaged sensor layout, (b) and the integrated sensors embedded in the composite tool. The middle part of the figure presents the optical microstructures integrated on chip.

OPTICS CONTINUUM

metal tube as described in [24,25]. The resulting temperature sensor probe can be seen in Fig. 3(a). The packaged sensors are embedded in the composite tool utilizing through thickness reinforcement (TTR) techniques [26], namely surrogate pinning, inserting dummy pins into the preform, substituting them with the packaged sensors after the end of the curing cycle. Figure 3(b) depicts the surface of the composite tool with the integrated optical sensor, exhibiting its small size (1 mm x 1 mm). At the middle part of the figure, the top-view of the silicon waveguide are visible.

2.2. Bragg grating design

In our previous work, the waveguided modes, and their associated effective index value (n_{eff}) of the Bragg grating design process were calculated using the finite difference eigenmode (FDE) computational tool of Lumerical commercial packages. As expected, the highest thermooptic coefficient of silicon can justify the high sensitivity in temperature change and as such, only TE structures were used in the testing phase. The electric field intensity distribution of a structure with a width of 450 nm and a height of 220 nm is shown in Fig. 4. It is also validated that the propagating TE mode has a high confinement into the silicon core.

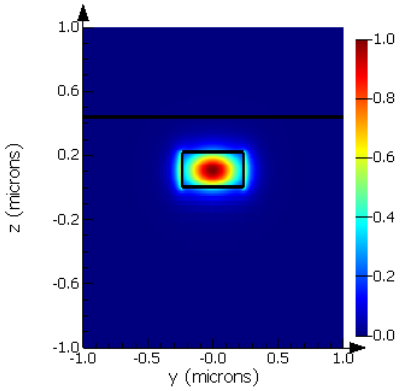

Fig. 4. Electrical field intensity distribution inside the Bragg grating waveguide.

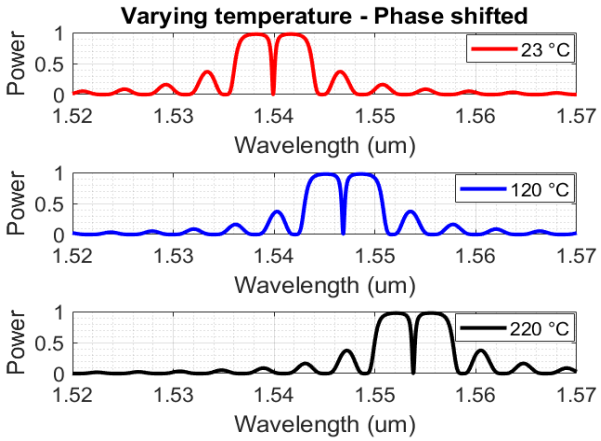

Fig. 5. Reflection spectra for phase shifted Bragg gratings of 328 nm, dw = 20 nm, N = 200 for temperatures of 23 °C, 120 °C and 220 °C.

OPTICS CONTINUUM

Following the waveguide modes calculation, a propagation simulation was by applying Lumerical's EME (eigenmode expansion) propagation solver. Utilizing the thermooptic modelling of silicon, with the refractive index varying according to its temperature, the results for the thermo-optic sensitivity (85 pm/°C [22]) are obtained. Figure 5 depicts the reflection lobes when temperature changes emerge in the Bragg grating with $\Lambda = 328$ nm and $dw = 20$ nm and 200 periods.

2.3. Experimental testbed

As an extension of previous work, Fig. 6 shows the steps of the experimental process including injection resin. The packaged sensor presented in the present work was initially characterized in a lab setup and the model produced from these measurements is then used to translate the dip in the reflection lobe, to a temperature value, after the resin infusion. This model is then used for a comparison to the thermocouple values, as well as the model produced by the optical-thermocouple measurements, in the curing phase.

It must be noted that the tool is self-heating eliminating the need for an oven or autoclave. The self-heating fabric – TIBGRID 110-ISO TTI-0.93 – is thin enough to be to be layered between the folds of benzoaxazine-preimpregnated fabric and co-cooked inside the skin. The epoxy resin used is an Epikote RIMR 035c/Epikure RIMH 037, from Westlake, with a curing temperature of 120°C. Next, the tool is heating with a temperature ramp to prepare the mold for the resin curing cycle. When the tool preparation is complete, the liquid resin is poured into the mold.

Throughout the process, an optical experimental setup comprised of a regular computer, a fiber interrogator, and an optical filtering configuration comprised of the polarizer and polarization controllers can acquire photonic data. For the temperature control of the heating process, electrical components (thermocouples) are utilized as well as for the calibration of the optical sensors, in a dry run setup. As the thermal resistivity of the composite tool complicates the

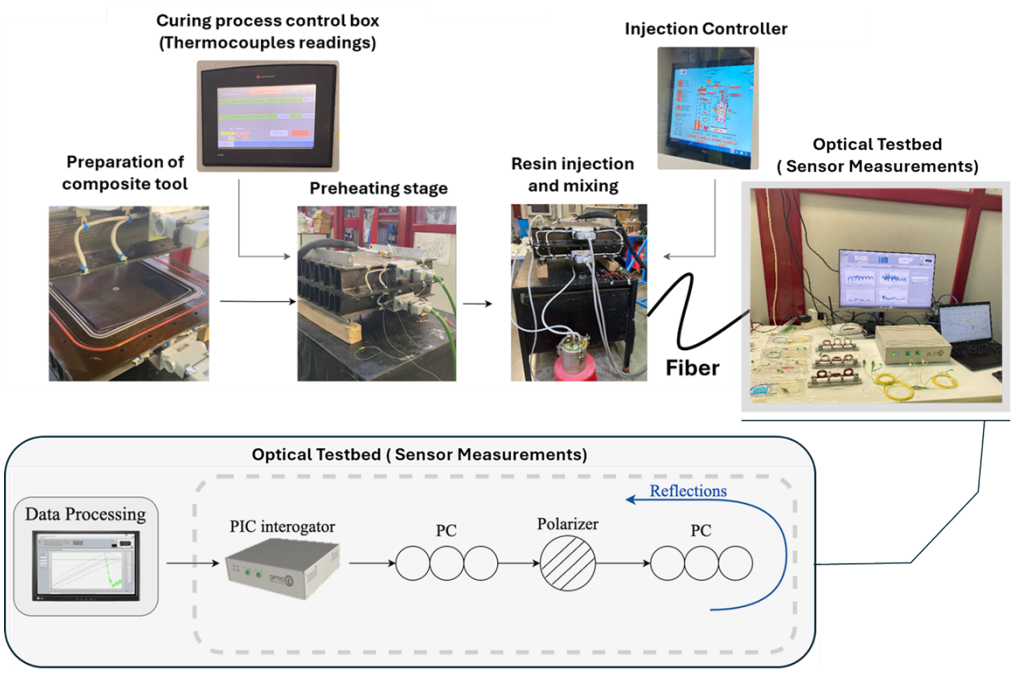

Fig. 6. Stages followed during the curing process.

OPTICS CONTINUUM

accurate control of the heating process, the required thermocouples are placed directly at the self-heating fabric, as shown in Fig. 7. After the initial calibration run in a dry run setup, the resin is infused inside the tool, and the temperature as assessed by the optical sensors, is compared to the thermocouple data.

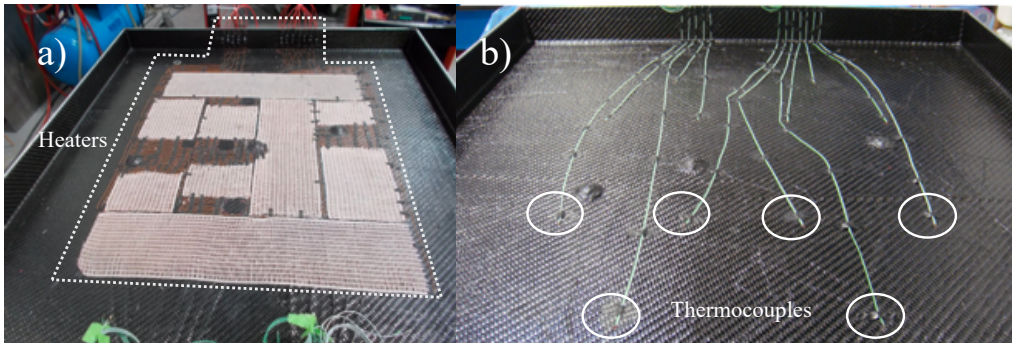

Fig. 7. Placing (a) heaters (b) thermocouples at the carbon-fibre fabric.

Specifically, the photonic structure is tested using commercial laser (2 mW) interrogator [27] (FAZT I4 G) to cover up to 39.2 nm in the C-band, reading the Bragg structure spectrum. It is important to emphasize that the interrogator provides a qualitative picture for the power measurements. This is not a critical limitation, as the wavelength shift is the main matter of interest.

When a dry run takes place for calibration purposes, the sensors are vacuum tested to ensure that they are capable of handling the pressure of resin injection over multiple cycles. In this study, the sensors are evaluated when a liquid resin infusion is included. The challenges of testing sensors during resin injection stem from the dynamic and demanding nature of the process, including pressure variations, material compatibility, abrasive conditions, temperature considerations, real-time monitoring requirements, sealing integrity, and the need for repeatability over multiple cycles. Addressing these challenges is essential to ensuring that the sensors can perform their monitoring functions in resin injection applications in an accurate and reliable way.

The data is processed using a second-type Chebyshev filter for high execution speed, allowing fast monitoring and control. The filter's passband and stopband frequencies are optimized, with attenuation set to 100 dB and 0.1 dB ripple.

3. Experimental results

This section presents the outcomes of the Bragg grating sensor from the spectra acquired during the dry run and curing processes. The initial dry run conditions are defined as test run status in which the Bragg grating sensor measures accurate temperature at a dynamic range of 35°C up to 100 °C, as shown in Fig. 8. It should be noted that the linear sensitivity of ≈ 0.075 nm/°C of Bragg sensor measured in lab conditions, is consistent with the results from the optical simulations reported in [22]. Starting at 35°C, a red-shift of 1.875 nm and 4.125 nm leads to a 25°C and 55°C difference, respectively. The sensor was calibrated up to 100°C using the reference thermocouple probe in close proximity to the sensor under test. Figure 9 demonstrates the initial calibration of the sensor, with the temperature as measured by the thermocouples (blue line) and the temperature as recorded by the optical sensors (red dots).

A difference from the simulated results must also be noted, namely the bandwidth of the reflection spectrum, and the reflection dip in particular. This effect can be attributed to deviations

OPTICS CONTINUUM

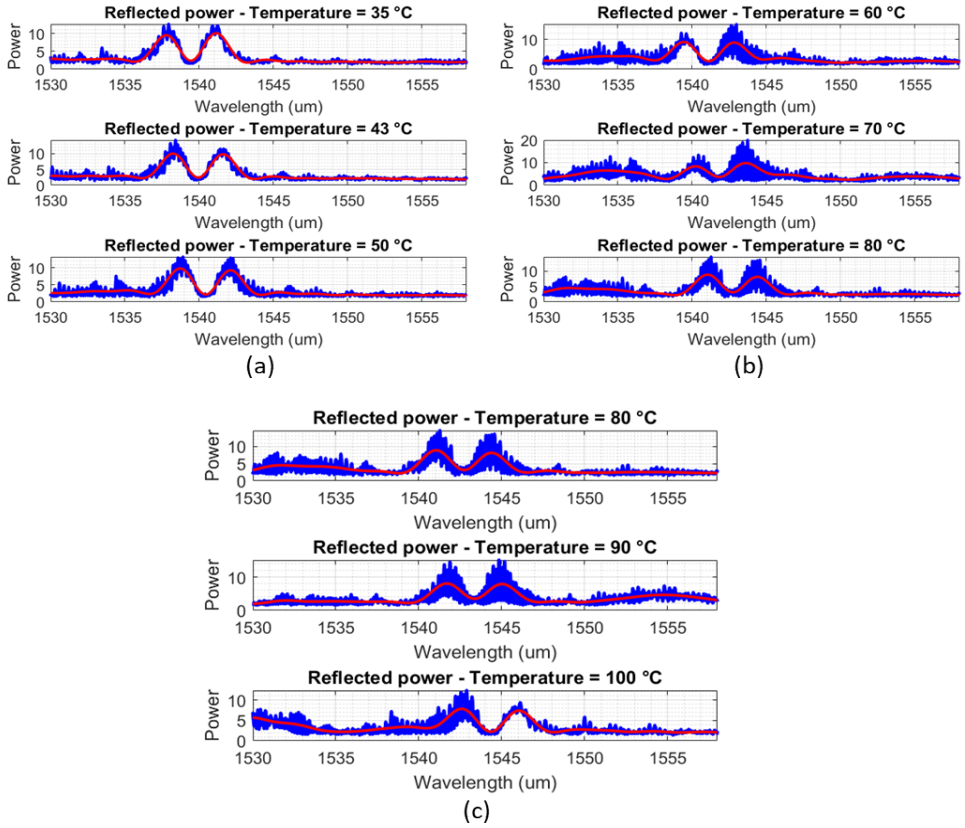

Fig. 8. Recorded reflection spectra for a Bragg grating sensor, at temperatures: (a), 35, 43, 50 (b) 60, 70 80, (c)` 80, 90 100°C.

of the structures due to fabrication, especially in the shape of the sidewall corrugations, as the gratings' edges become smoother [28], due to diffraction effects in the photomask.

It is also worthy of mention that the wavelength of the dip of the reflection lobe is assigned to the temperature value obtained by the thermocouples. This alignment between the Bragg grating sensor and thermocouple readings of the in-tool dry characterization during heating time is then used for the curing process measurements.

The reflection spectra of a second embedded sensor are presented in Fig. 10, in a dry run setup with a temperature range close to room temperature conditions (30-40°C). The sensor is sensitive to misalignments between the chip and the optical fiber, and the signal was lost beyond that range.

The resin cure state is achieved in the second part under the application of a specific heating cycle. Figure 11(a) and (b) reveal the reflection spectra at multiple temperature values after the resin infusion (90°C up to 120°C). As before, the shifting of wavelength confirms this temperature difference. Figure 12 provides the temperature as measured by the optical sensors (red dots) and the thermocouples (blue line). The x-axis represents the time of the curing process, including the ramp stage (from 70°C to 90°C), the injection (90°C) and the curing phase (after 90°C). The total difference between the optical and electrical (thermocouple) values is determined at 1-5% and is demonstrated as the yellow bars. This disparity is due to the location of the sensors, with the thermocouples being installed near the heaters while the optical sensors are located right at the edge of the tool, therefore sensing the resin's condition with higher fidelity.

OPTICS CONTINUUM

Lastly, Fig. 13 compares the linear model of the sensor' dry calibration (R^2=0.995), with the sensing during injection and curing stage and its fitted model (R^2=0.988). The y-axis represents the Bragg resonance of the sensors, i.e. the wavelength of the dip in the reflection lobe with the x-axis demonstrating the temperature. The obtained response of the regression model during resin injection, proves the existence of small but noticeable temperature discrepancies, between the resin and the thermocouples used for heating control, as the thermal conductivity of epoxy resins (0.15–0.25 W/mK) [29] is an order of magnitude higher than that of air (0.026 W/mK) [30]. Finally, there was no apparent shift of the photonic sensors at the same temperature, before and after the injection, i.e. after the heating-up, vacuum was induced to assist the injection, something that was not recorded by the photonic sensors. These results are reinforcing the need for the deployment of miniaturized optical sensors at the edge of the tool, closely monitoring the curing temperature of the resin.

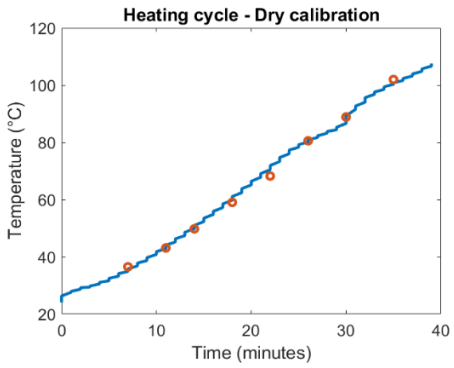

Fig. 9. The optical sensor calibration up to 100 °C regarding thermocouple data during in-tool dry characterization.

OPTICS CONTINUUM

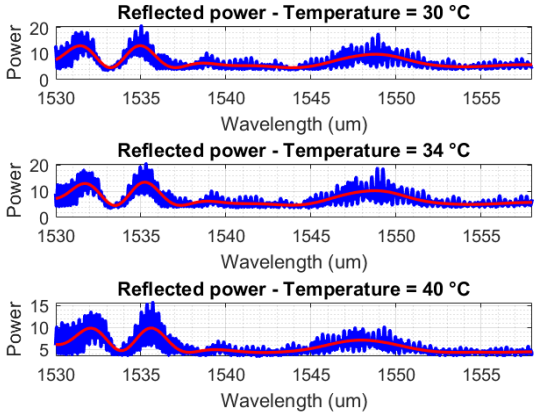

Fig. 10. Reflection spectra of a second sensor, embedded in the composite tool, for 30, 34 and 40°C, for a dry run setup.

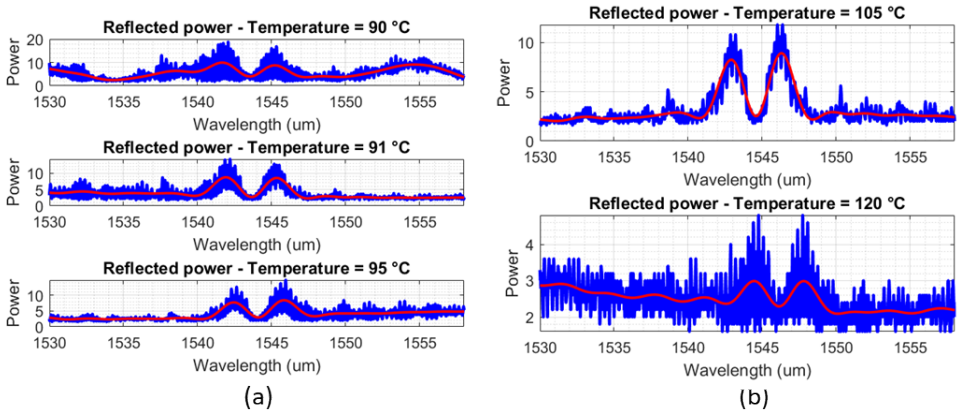

Fig. 11. Recorded reflection spectra for a Bragg grating sensor, at temperatures: (a), 90, 91, 95 (b) 105, 120°C, after the resin injection.

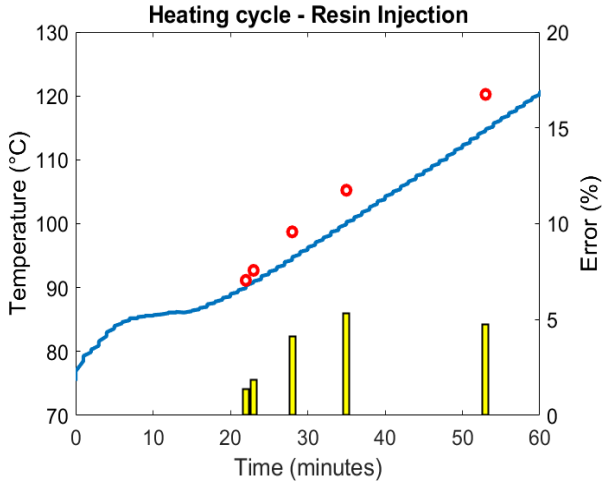

Fig. 12. Comparison of thermocouple and Bragg grating sensor temperature measurements during the resin curing process after the 80 °C.

OPTICS CONTINUUM

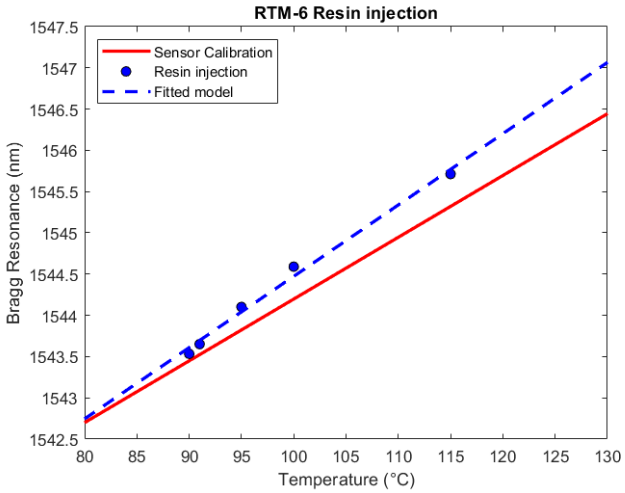

Fig. 13. Sensor calibration (red line), resin temperature (blue line) as measured by the optical sensor and its fitted model curves (blue dotted line).

OPTICS CONTINUUM

4. Conclusions

This study demonstrates the successful integration and proof of concept demonstration of a photonic integrated circuit (PIC) based on a 220 nm height Silicon-on-Insulator platform for in-situ monitoring of the temperature during the resin curing process in composite tools. The small size, electromagnetic immunity and fast response of the photonic structures enable the accurate monitoring of resin curing cycles. The embedded phase-shifted Bragg grating sensors exhibit high sensitivity (75 pm/°C) and linearity (R^2=0.995), operating up to 120 °C, allowing precise temperature measurements throughout the curing cycle. The optical sensors went through calibration, dry run characterization, and curing process measurements, with the small variations in measurement caused by the local temperature profile in the tool-resin interface. The experimental results validate the effectiveness of the proposed Bragg grating sensor, while also highlighting its constraints, making it a promising solution for measuring accurate temperature in advanced composite manufacturing processes such as resin transfer molding (RTM).

Funding. Horizon 2020 Framework Programme (101017186).

Acknowledgments. The authors want to express their appreciation in the efforts of Santiago Miguel Aznar and Fernando Soria for their crucial contribution and assistance in the execution of the experiments.

Disclosures. The authors declare no conflict of interest.

Data availability. The data that support the findings of this study are available from the corresponding author, G.S., E.K. upon reasonable request.

References

1. C. Soutis, "Fibre reinforced composites in aircraft construction," Prog. Aerosp. Sci. **41**(2), 143–151 (2005).
2. S. Laurenzi and M. Marchetti, "*Advanced Composite Materials by Resin Transfer Molding for Aerospace Applications*," in N. Hu, eds. (InTech, 2012).
3. S. S. J. Roberts and R. Davidson, "Cure and fabrication monitoring of composite materials with fibre-optic sensors," Compos. Sci. Technol. **49**(3), 265–276 (1993).
4. P. R. N. Childs, J. R. Greenwood, and C. A. Long, "Review of temperature measurement," Rev. Sci. Instrum. **71**(8), 2959–2978 (2000).
5. M. Mieloszyk, K. Majewska, and W. Ostachowicz, "Application of embedded fibre Bragg grating sensors for structural health monitoring of complex composite structures for marine applications," Mar. Struct. **76**, 102903 (2021).
6. C. Ciminelli, F. Dell'Olio, C. E. Campanella, *et al.*, "Photonic technologies for angular velocity sensing," Adv. Opt. Photonics **2**(3), 370–404 (2010).
7. P. Roriz, O. Frazão, A. B. Lobo-Ribeiro, *et al.*, "Review of fiber-optic pressure sensors for biomedical and biomechanical applications," J. Biomed. Opt. **18**(5), 050903 (2013).
8. K. Bohnert, P. Gabus, J. Kostovic, *et al.*, "Optical fiber sensors for the electric power industry," Opt. Lasers Eng. **43**(3-5), 511–526 (2005).
9. S. Young, D. Penumadu, A. D. Patchen, *et al.*, "Smart polymer composite deck monitoring using distributed high definition and Bragg grating fiber optic sensing," Sensors **22**(11), 4089 (2022).
10. D. C. Betz, G. Thursby, B. Culshaw, *et al.*, "Identification of structural damage using multifunctional Bragg grating sensors: I. Theory and implementation," Smart Mater. Struct. **15**(5), 1305–1312 (2006).
11. P. Ferdinand, S. Magne, V. Dewynter-Marty, *et al.*, "Applications of fiber Bragg grating sensors in the composite industry," MRS Bull. **27**(5), 400–407 (2002).
12. D. C. Betz, L. Staudigel, M. N. Trutzel, *et al.*, "Structural monitoring using fiber-optic Bragg grating sensors," Struct. Health Monit. **2**(2), 145–152 (2003).
13. D. Kinet, P. Mégret, K. W. Goossen, *et al.*, "Fiber Bragg grating sensors toward structural health monitoring in composite materials: challenges and solutions," Sensors **14**(4), 7394–7419 (2014).
14. A. Papantoniou, G. Rigas, and N. D. Alexopoulos, "Assessment of the strain monitoring reliability of fiber Bragg grating sensor (FBGs) in advanced composite structures," Compos. Struct. **93**(9), 2163–2172 (2011).
15. J. F. Tao, H. Cai, Y. D. Gu, *et al.*, "Demonstration of a Photonic-Based Linear Temperature Sensor," IEEE Photon. Technol. Lett. **27**(7), 767–769 (2015).
16. G.-D. Kim, H.-S. Lee, C.-H. Park, *et al.*, "Silicon photonic temperature sensor employing a ring resonator manufactured using a standard CMOS process," Opt. Express **18**(21), 22215–22221 (2010).
17. V. M. N. Passaro, C. D. Tullio, B. Troia, *et al.*, "Recent advances in integrated photonic sensors," Sensors **12**(11), 15558–15598 (2012).
18. N. L. Kazanskiy, S. N. Khonina, and M. A. Butt, "Advancement in silicon integrated photonics technologies for sensing applications in near-infrared and mid-infrared region: a review," Photonics **9**(5), 331 (2022).

OPTICS CONTINUUM

19. D. Melati, A. Alippi, and A. Melloni, "Reconfigurable photonic integrated mode (de)multiplexer for SDM fiber transmission," Opt. Express **24**(12), 12625–12634 (2016).
20. G. Syriopoulos, A. Poulimenos, G. Poulopoulos, *et al.*, "Demonstration of photonic temperature sensor for RTM-6 composite manufacturing process (180°C) integrated with PMOC system," in *Integrated Optics: Devices, Materials, and Technologies XXVII* (SPIE, 2023), Vol. 12424.
21. I. Poulopoulos, C. Zervos, G. Syriopoulos, *et al.*, "Silicon photonics temperature and refractive index sensor for curing process monitoring in composite material industry," in *Optical Sensing and Detection VII* (SPIE, 2022), Vol. 12139, pp. 76–88.
22. G. Syriopoulos, I. Poulopoulos, C. Zervos, *et al.*, "Photonic Integrated Circuit Based Temperature Sensor for Out-of-Autoclave Composite Parts Production Monitoring," Sensors **23**(18), 7765 (2023).
23. F. J. Ferraro, P. D. Heyn, M. Kim, *et al.*, "Imec silicon photonics platforms: performance overview and roadmap," in *Next-Generation Optical Communication: Components, Sub-Systems, and Systems XII* (SPIE, 2023), Vol. 12429, pp. 22–28.
24. J. Missinne, V. Geudens, S. Van Put, *et al.*, "A fully packaged silicon photonic Bragg grating temperature sensor with a compact back side interface based on a ball lens," in *Silicon Photonics XVIII*, G. T. Reed and A. P. Knights, eds. (SPIE, 2023), p. 27.
25. J. Missinne, V. Geudens, G. Poulopoulos, *et al.*, "Silicon photonic temperature sensor: from photonic integrated chip to fully packaged miniature probe," J. Opt. Microsyst. **4**(01), 011005 (2023).
26. G. Neale and A. Skordos, "Insertion of large diameter through-thickness metallic pins in composites," Mater. Des. **216**, 110559 (2022).
27. S. K. Ibrahim, M. Farnan, D. M. Karabacak, *et al.*, "Enabling technologies for fiber optic sensing," in F. Berghmans and A. G. Mignani, eds. (2016), p. 98990Z.
28. X. Wang, W. Shi, R. Vafaei, *et al.*, "Uniform and sampled Bragg gratings in SOI strip waveguides with sidewall corrugations," IEEE Photon. Technol. Lett. **23**(5), 290–292 (2011).
29. S.-L. Chung and J.-S. Lin, "Thermal conductivity of epoxy resin composites filled with combustion synthesized h-BN particles," Molecules **21**(5), 670 (2016).
30. B. Graczykowski, A. El Sachat, J. S. Reparaz, *et al.*, "Thermal conductivity and air-mediated losses in periodic porous silicon membranes at high temperatures," Nat. Commun. **8**(1), 415 (2017).